International Journal of Nanomedicine

Dovepress

open access to scientific and medical research

Open Access Full Text Article

ORIGINAL RESEARCH

Procedural Promotion of Wound Healing by Graphene-Barium Titanate Nanosystem with White Light Irradiation

Jianlin Wang*, Zhaoyang Wen*, Yumei Xu, Xin Ning, Deping Wang, Jimin Cao, Yanlin Feng

Key Laboratory of Cellular Physiology at Shanxi Medical University, Ministry of Education, and the Department of Physiology, Shanxi Medical University, Taiyuan, 030001, People's Republic of China

*These authors contributed equally to this work

Correspondence: Yanlin Feng; Jimin Cao, Email feng@sxmu.edu.cn; caojimin@sxmu.edu.cn

Background: Wound healing is a continuous and complex process that comprises multiple phases including hemostasis, inflammation, multiplication (proliferation) and remodeling. Although a variety of nanomaterials have been developed to control infection and accelerate wound healing, most of them can only promote one phase but not multiple phases, resulting in lower efficient healing. Although various formulations such as nitric oxide releasing wound dressings were developed for dual action, the nanostructure synthesis and the encapsulation process were complex.

Materials and Methods: Here, we report on the design of graphene-barium titanate nanosystem to procedural promote the wound healing process. The antibacterial effect was assessed in Gram-negative *Escherichia coli* bacteria (*E. coli*) and Gram-positive *Staphylococcus aureus* bacteria (*S. aureus*), the cell proliferation and migration experiment was investigated in mouse embryonic fibroblast (NIH-3T3) cells, and the wound healing effect was analyzed in female BALB/c mice with infected skin wound on the back.

Results: Results showed that graphene-barium titanate nanosystem could generate abundant ROS to kill both *E. coli* and *S. aureus*. The growth curves, bacterial viability, colony number formation and scanning electron microscopy (SEM) images of *E. coli* and *S. aureus* all confirmed the antibacterial effect. Cell Counting Kit-8 (CCK-8) assay displayed that GBT possesses great biocompatibility. EdU assay showed that GBT plus white light irradiation significantly promoted the proliferation and migration of NIH-3T3 cells. Scratch assay found that GBT could achieve a fast scratch closure compared to the control. In vivo wound healing effect indicates that GBT can accelerate wound repair procedure.

Conclusion: GBT nanocomposite is capable of programmatically accelerating wound healing through multiple stages, including production of a large amount of ROS after white light exposure to effectively kill *E. coli* and *S. aureus* to prevent wound infection and as a scaffold to accelerate fibroblast proliferation and migration to the wound to accelerate wound healing.

Keywords: graphene-barium titanate nanosystem, wound healing, reactive oxygen species, antibacterial, proliferation

Introduction

Skin is the largest organ of our body, and as the first immune barrier, it protects the body from pathogens at all times. Skin is also vulnerable to various threats, and skin damage and wound formation are common in response to external detrimental stimuli. Wound healing is a complex dynamic process that compromises multiple stages including hemostasis, inflammation, multiplication and remodeling.[1–3] After skin damage, the hemostasis phase occurs immediately, aiming to quickly stop bleeding. Hemostasis is caused by blood vessel constriction and platelet accumulation and coagulation at the vascular wound and to form a protective barrier to prevent external pathogens entering the bloodstream.[4] Inflammation phase is the secondary stage of wound healing. In this phase, the wound is susceptible to bacterial infection, which may lead to inefficient healing.[5] The immune system is activated in this phase to trigger inflammation aiming to inhibit bacterial growth and wound infection, thus accelerating the process of wound healing. Multiplication phase is the third stage of wound healing and is the key step in

Received: 21 February 2023
Accepted: 31 July 2023
Published: 7 August 2023

wound healing. In this phase, endothelial cells and other cells such as fibroblasts and epidermal cells proliferate and migrate to form new blood vessels and new tissues gradually covering the wound.[6] Remodeling phase is the fourth stage of wound healing, wound is completely closed and new epithelium and scar are formed in this phase.[7] Wound healing requires that all stages are coordinated, and if any stage is not carried out normally, it will lead to delay of the healing process.

How to promote wound healing is still an important but not well-solved medical issue. In recent years, nanotechnology has shown its superiority in promoting wound healing. Various nanomaterials, including silver nanoparticles,[8] graphene quantum dots,[9] cerium dioxide,[10] and copper metal-organic framework hydrogel,[11] are widely used to accelerate wound healing. However, most of them can only promote a single phase, such as the infection or multiplication phase, but are unable to programmatically promote multiple phases to achieve effective wound healing. Although various formulations such as nitric oxide releasing wound dressings were developed for dual action,[12,13] the nanostructure synthesis and the encapsulation process were complex. Therefore, there is a need to develop new easily synthesized nanosystems with simple composition, compact structures but multiple functions, and capable of accelerating wound healing by regulating multiple stages of wound healing. Barium titanate ($BaTiO_3$, BT), as a classic ferroelectric semiconductor material, has been proved useful in the field of biomedicine.[11,14,15] However, the failure to prevent the rapid recombination of electron and hole reduces the efficiency of ROS.[16–18] Graphene (G) has attracted wide interest because of its excellent electronic, mechanic, and optical properties that could be used for both physical and chemical antibacterial activity.[19] Physical damage mainly contributes from its large surface area and sharp edges. The large graphene nanosheet would entrap the bacteria to prevent the nutrient supply to starve the bacteria, while the sharp edges would penetrate the bacterial membranes to extract phospholipid molecules destructively, and then damage RNA to exert antimicrobial effect.[20–24] Chemical damage is caused by oxidative stress or by charge transfer.[25–28] In the proliferation and remodeling stages, extensive research has showed that graphene could act as scaffold for cell proliferation and migration.[29–33] Thus, a combination of graphene and BT may enhance the antibacterial effect under white light irradiation, which can accelerate wound healing by inhibiting the inflammation phase and accelerating the multiplication phase.

In this work, we designed and synthesized the GBT nanosystem which is able to kill bacteria and promote wound healing. At the inflammation phase, the separation of electron-hole pairs from BT and graphene could induce the production of a large amount of ROS after white light exposure, which could effectively kill *E. coli* and *S. aureus* to prevent wound infection. At the proliferation phase, graphene could act as a scaffold to accelerate fibroblast proliferation and migration to the wound to accelerate wound healing. With simple composition, compact structures but multiple functions, GBT nanosystem could accelerate the inflammation and proliferation stages of wound healing.

Materials and Methods

Materials

Barium titanate (99%), hydrogen peroxide (H_2O_2), (3-aminopropyl)triethoxysilane (APTES) (99%), dimethylaminopropyl)-3-ethylcarbodiimide hydrochloride (EDC) and N-hydroxysuccinimide (NHS) were obtained from Aladdin. Single-layer graphene was purchased from MACKLIN. All of these reagents were used without any further purification. Ultra-pure water used in all experimental procedures was obtained from a Milli-Q water purification system.

Fabrication of Amino Groups (NH_2)-Functionalized $BaTiO_3$ (BT-NH_2)

Four hundred milligrams of BT was dispersed in 25 mL of hydrogen peroxide solution by sonication for 20 min in a 50-mL flask. The solution was kept at 110 °C for 4 h under reflux with stirring at 750 rpm. After the reaction, the solution was centrifuged at 10,000 rpm for 5 min and then washed with water and ethanol 2 times, respectively. After discarding the supernatant, the solid pellets were dispersed in ethanol. Four hundred microliters APTES solution was added to the above solution and stirred for 24 h at 80 °C. The resulted powder was finally washed with water instead of ethanol. The as designed compound was referred to as BT-NH_2.

Synthesis of GBT

About 100 mg of graphene was dispersed in 80 mL ultrapure water, and 10 mM of EDC and 25 mM of NHS were added to the solution and stirred for 15 min at 30 °C. Then, 100 mg of $BaTiO_3$-NH_2 was mixed with the solution. The final

solution was stirred overnight away from light. The resulted nanoparticles were centrifuged at 10,000 rpm for 5 min and washed twice with water to obtain GBT.

Detection of ROS Production by GBT in vitro

Total ROS generation of GBT was detected by 2′,7′-dichlorodihydrofluorescein diacetate (H2DCFDA) assay. We added 80 μL of 10 μM DCF working solution and 20 μL GBT (400 μg/mL) to each well of a 96-multiwell plate, followed by 30 min of white light irradiation or not. After another 2 hours of incubation, DCF fluorescence emission spectra were collected with an excitation wavelength of 490 nm. Hydroxyl radical (HO•) was detected by 3′-(p-aminophenyl) fluorescein (APF) (10 μM). Then, 80 μL of 10 μM APF was mixed with 20 μL of 400 μg/mL GBT, and the same assay was performed. APF fluorescence emission spectra were detected with an excitation wavelength of 480 nm.

Evaluation of the Antibacterial Activity of GBT in vitro

Gram-negative *E. coli* and Gram-positive *S. aureus* were used to the models in the study. The two kinds of bacteria were grown in a liquid Luria-Bertani (LB) culture medium at 37 °C for 12 h under 220 rpm rotation. The concentration of bacteria was detected by measuring the optical density of the suspension at 600 nm (OD_{600}). The bacteria grew to 1×10^8 colony forming units per milliliter (CFU/mL) when the value of optical density at 600 nm (OD_{600}) increased to 0.5. *E. coli* and *S. aureus* bacterial suspensions were mixed with GBT suspension, resulting in various concentrations of GBT (0, 12.5, 25, 50, 100, 200, 400, and 800 μg/mL). The mixed solution was incubated in each well of a 96-multiwell plate and irradiated with white light for 30 min at a density of 0.1 W/cm^2 or not. Then, the bacteria were incubated for 6 h at 37 °C under 220 rpm rotation. The absorption value at 600 nm was detected every 1 h, and the growth curve was made. After 6 h, the resulting solution was diluted 10,000 times and then 50 μL of the solution were spread on agar plate. After 24 h of growing at 37 °C, the images of the bacterial colonies were recorded.

SEM was used to observe the changes of bacterial morphology. Bacteria suspension (150 μL, 2×10^7 CFU/mL) was mixed with 50 μL of 2.4 mg/mL GBT suspension. The resulting suspension was irradiated with 0.1 W/cm^2 white light or not for 30 min, followed by 24 h of incubation at 37 °C on a rotary platform at a 180 rpm. After centrifugation, the bacteria were collected by centrifugation at 3,000 rpm for 5 min. Then, the bacteria were washed with PBS and fixed with 2.5% glutaraldehyde solution at 4 °C overnight. After 3 washes with PBS and dehydration by ethanol gradient, SEM images of the bacteria were captured.

Detection of Bacterial ROS Generation

Bacteria suspension (150 μL, 2×10^7 CFU/mL) was mixed with 50 μL of 2.4 mg/mL GBT suspension. The resulting suspension was irradiated with 0.1 W/cm^2 white light or not for 30 min. After incubation at 37 °C for 6 h under 220 rpm rotation, 80 μL of DCF working solution (10 μM) was added into the above resulting solutions and incubated for 30 min in the darkness. Finally, the bacterial solution was washed twice with PBS and placed the liquid on the glass slide to image by fluorescence microscope.

Cell Culture

Mouse embryonic fibroblast (NIH-3T3) cells were purchased commercially from Shanghai Zhong Qiao Xin Zhou Biotechnology Co., Ltd. (Shanghai, China) and cultured in high-glucose Dulbecco's modified Eagle's medium (DMEM) supplemented with 10% calf serum and 1% penicillin-streptomycin at 37 °C in a humidified 5% CO_2 atmosphere. The culture medium was refreshed every day, and the cells were passaged by trypsinization before confluence.

Cell Viability Assay

The viability of NIH 3T3 cells was detected by a Cell Counting Kit-8 (CCK-8) assay. About 1×10^4 3T3 cells in 100 μL culture medium were placed in each well of a 96-multiwell plate. After 24 h of incubation, the culture medium was replaced with 100 μL of fresh medium containing different concentrations of GBT (0.78, 1.56, 3.125, 6.25, 12.5, 25, 50, and 100 μg/mL). After treatment with GBT for 24 h, the cell viability was accessed by CCK-8 assay.

Cell Proliferation Assay

The proliferation ability of NIH 3T3 cells was tested using a cell proliferation assay kit (kFluor488-EdU) (KeyGEN BioTECH, Jiangsu Province, China) according to the manufacturer's instructions. About 100 μL of culture medium containing 1×10^4 3T3 cells was added to each well of a 96-multiwell plate. The medium was replaced with 100 μL of fresh medium containing 100 μg/mL GBT after 24 h. After 24-h treatment, cells were incubated with 10 μM EdU for 2 h. Cells were then incubated with Click-iT reaction mixture for 30 min at the temperature without light. Afterwards, cells were co-cultured with 5 μg/mL Hoechst 33342 for 30 min at the temperature. Cell fluorescent images were captured with a microscope (Olympus; Tokyo, Japan).

Scratch Assay

About 1.6×10^6 NIH 3T3 cells were placed into a 6-well plate to let to grow. After 24-h culture, a scratch of 320 μm wide was created in the each well, followed by washing for three times with phosphate buffer saline (PBS). The culture medium was replaced with the fresh medium. Then, 100 μg/mL GBT was added to the medium and the culture was continued for 24 h. Finally, digital images were captured at 24 h after GBT incubation. The percentages of wound healing were analyzed using ImageJ software.

In vivo Wound Repair Experiments

Female BALB/c mice with age of 4–6 weeks old and body weight of about 20 g were purchased from Center for Experimental Animals, Shanxi Medical University. The back of the mice was first unhaired and sterilized with 75% ethanol at a local site. Then, a circular, full-thickness skin wound of about 10 mm in diameter was created with a surgical knife. Then, the wounds were infected by *E. coli* suspension (10 μL, 1×10^8 CFU/mL) and the moisture allowed to evaporate naturally. To confirm the success of infection, bacterial samples were collected from the wound by sterilized cotton swabs at 2 h post-infection or 7 days post-management. Swabs were immersed in 1 mL normal saline solution. After incubating *E. coli* on LB agar plates at 37 °C for 24 hours, typical streaking plating method was used to investigate alive *E. coli* in the diluted suspension. The bacterial colonies were imaged for analysis. Then, the mice were divided into four groups: Control, GBT, Light, and GBT + Light. For the GBT + Light treatment group, 50 μL of GBT (100 μg/mL) was dropped onto the wound, then the wound was exposed to light irradiation (0.1 W/cm^2) for 20 min. Similarly, the other three groups were administered using the same procedure. The wounds were imaged, and wound sizes were measured every 2 days.

After 8 days of treatment, mice were sacrificed and tissues surrounding the wounds were harvested, routinely developed, embedded in paraffin, and sectioned with a microtome. Wound tissue section of 5 μm was stained with hematoxylin and eosin (H&E) and Masson's trichrome. Images were taken using a light microscope. The procedures involving experimental animals were in accordance with protocols approved by the Committee for Shanxi Medical University and were in accordance with the guidelines for the Care and Use of Laboratory Animals (NIH, revised 2011). The approval number of animal ethics is SYDL2019012.

Statistical Analysis

Data were presented as mean or mean ± standard deviation (SD). Statistical significance was determined using One-Way ANOVA. The difference was considered statistically significant when $p < 0.05$.

Results and Discussion

Fabrication and Characterization of GBT

GBT was sequentially synthesized in several steps. BT nanospheres about 34 nm were purchased (Figure 1A). The graphene was prepared through Hummers method (Figure 1B).[34] Then, amino groups (NH_2) were introduced into BT nanospheres through hydrolysis of APTES after it was saturated with hydroxyl groups using hydrogen peroxide. Lastly, GBT was formed by coupling the amino groups of BT with the carboxyl groups of graphene through NHS/EDC coupling. Transmission electron microscopy (TEM) images of GBT (Figure 1C) showed that BT was distributed onto the surface of

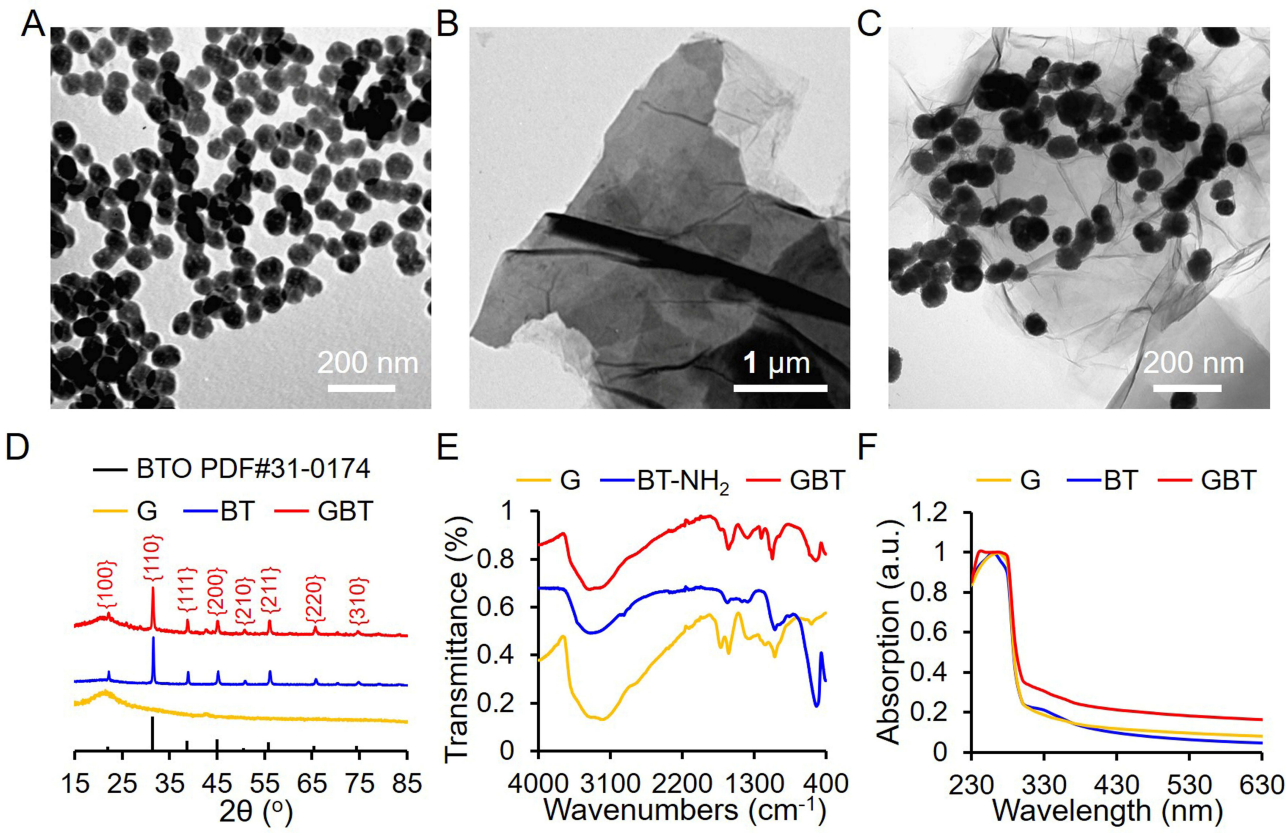

Figure 1 Characterization of GBT. (**A**–**C**) TEM images of G, BT, and GBT. (**D**) The XRD pattern of GBT. (**E**) The FTIR spectra of G, BT, and GBT. (**F**) The UV-vis spectra of G, BT, and GBT. White light spectrum ranging from 200 to 1000 nm.

graphene. The existence of BT in graphene was confirmed by X-ray diffraction (XRD) patterns (Figure 1D). The surface functionalization of BT with amino groups was characterized using Fourier transform infrared spectroscopy (Figure 1E). For BT-NH_2, the amine N-H bending band at around 1630 cm^{-1} and the internal vibration of amide bond peak at around 1380 cm^{-1} indicated the success of the surface modification process. It further demonstrated successful conjugation of BT to graphene. Moreover, the UV–vis absorbance spectra (Figure 1F) demonstrated the optical properties of G, BT, and GBT, which reveal that the light absorption capacity of GBT was greatly enhanced in the white light region compared to pure BT and G.

The ROS Generating and Antibacterial Abilities of GBT Under Simulated Sunlight Irradiation

The ROS generation ability of GBT was assessed by H2DCFDA assay. Under white light irradiation, the DCF fluorescence intensity of GBT was higher than PBS and GBT without white light irradiation, indicating that GBT could generate more ROS than other groups under white light irradiation (Figure 2A). We further detected the type of ROS generated by GBT using APF assay under white light irradiation. Result showed that GBT had the highest APF fluorescence intensity, suggesting that HO• is the main type of ROS (Figure 2B). Moreover, the generation ability of total ROS and HO• of GBT was concentration dependent (Figure 2C and D).

Nanomaterials with abundant ROS generation ability can result in inactivation of bacteria because ROS can damage a series of cell organelles and bio-macromolecule, such as cell membrane, lipids, protein, and nucleic acids.[35–37] To examine the antibacterial ability of GBT, we utilized Gram-negative *E. coli* and Gram-positive *S. aureus* to assess the bacteria growth kinetics at 0−6 h with or without white light irradiation. *E. coli* and *S. aureus* were incubated with (0–800 μg/mL) GBT for 2 h under the irradiation with white light (0.1 W/cm^2, 30 min), and then monitor the bacteria growth over 6 h by measurement of the optical

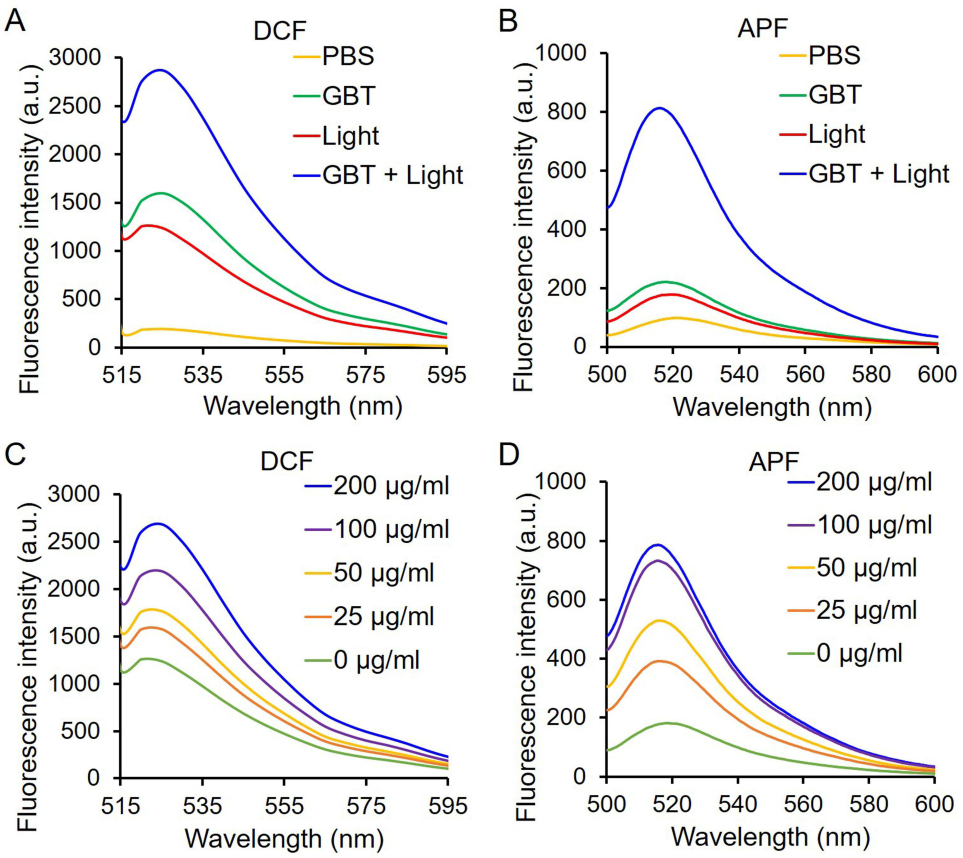

Figure 2 The ROS-generating abilities of GBT. (**A** and **B**) Total ROS and HO• generation ability of GBT with or without white light irradiation assessed by DCF and APF assay, respectively. (**C** and **D**) Assessments of total ROS and HO• of GBT with various concentrations. PBS was used as a control. PBS was used as a control.

density of bacteria at 600 nm. Figure 3A and B illustrated that under white light irradiation, GBT remarkably suppressed the growth of both types of bacteria, indicating that GBT had outstanding antibacterial ability and this ability was concentration-dependent. However, GBT could not exert inhibitory effect on bacteria growth without white light irradiation (Figure 3C and D). Figure 3E and F demonstrated that bacterial viability was gradually reduced with the increasing concentration of GBT with white light irradiation. Similarly, without white irradiation, no reduction in bacterial viability was observed in *E. coli* and *S. aureus* bacteria.

The bacteria growth inhibition performances were also assessed by observing the number of colony-forming units on Luria−Bertani (LB) agar plates after treated with GBT of different concentrations. It was found that under white light irradiation, GBT-treated bacteria showed significantly reduced colony number in a dose-dependent manner (Figure 4A), while white light or GBT alone could not cause the bacterial death (Figure 4B). Taken all together, we found the antibacterial activity of GBT is proportional to the ROS generation, proving the intense relationship between ROS production and antibacterial activity of GBT.

Mechanism of the Antibacterial Effect of GBT

The close relationship between ROS production and antibacterial activity suggests that abiotic ROS production on GBT could give rise to induction of cellular ROS generation in bacteria. As a result, we hypothesized that ROS generation was the leading mechanism underlying the antibacterial activity of GBT. To identify the existence of ROS inside the bacteria, we measured the level of ROS production within bacteria using H2DCFDA assay on a confocal laser scanning microscope (CLSM). Under white light irradiation, GBT significantly enhanced the bacterial DCF fluorescence, while white light or GBT

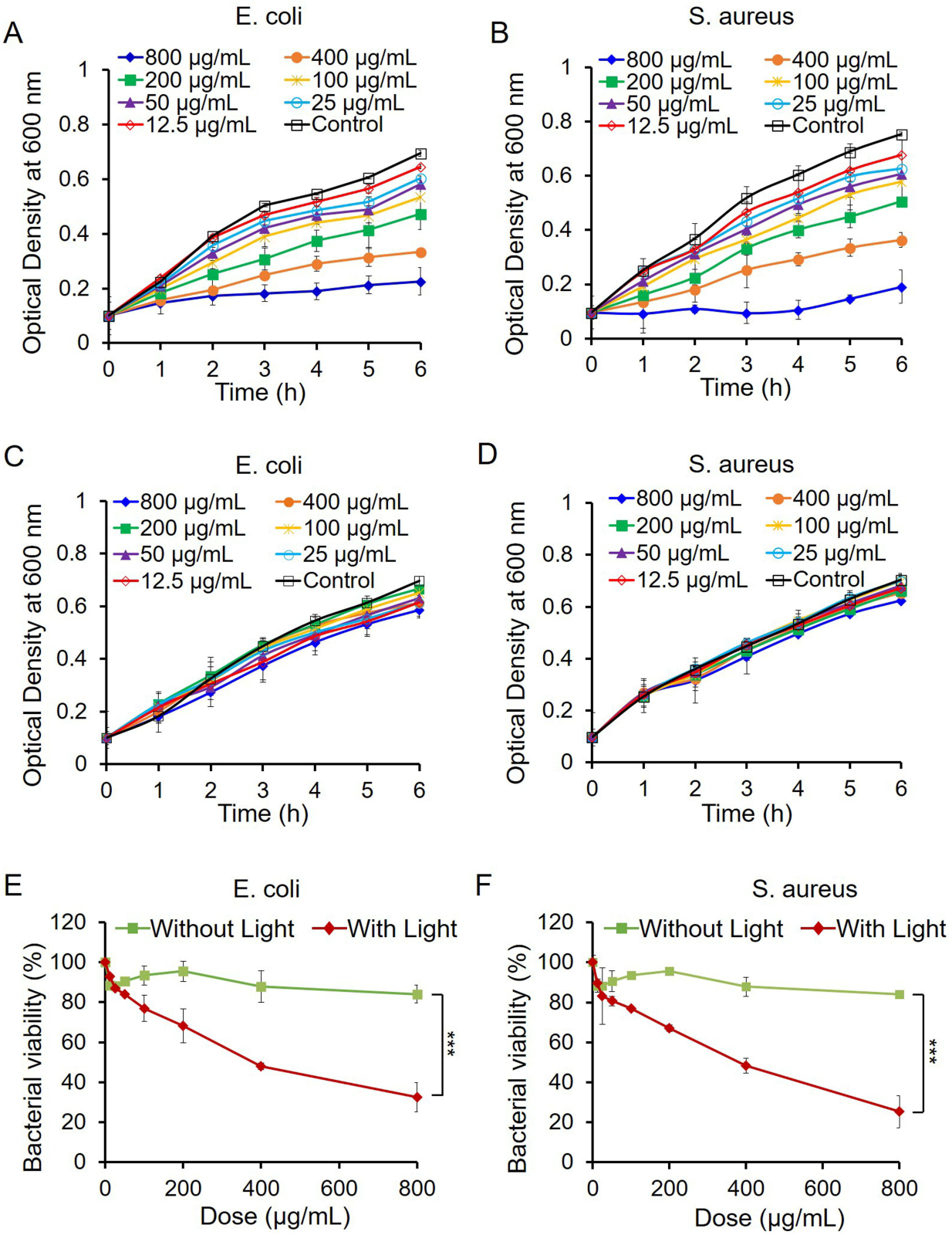

Figure 3 The anti-bacterial abilities of GBT. The growth curves of *E. coli* (**A** and **C**) and *S. aureus* (**B** and **D**) treated by different concentrations of GBT with (**A** and **B**) or without white light irradiation (**C** and **D**) within 6 h. Bacterial viability of *E. coli* (**E**) and *S. aureus* (**F**) exposed to different concentrations (0–800 μg/mL) of GBT for 6 h with or without white light irradiation. The bacteria viability was determined by comparing the optical density (at 600 nm) of GBT-treated bacteria with that of untreated bacteria. *** $p < 0.001$.

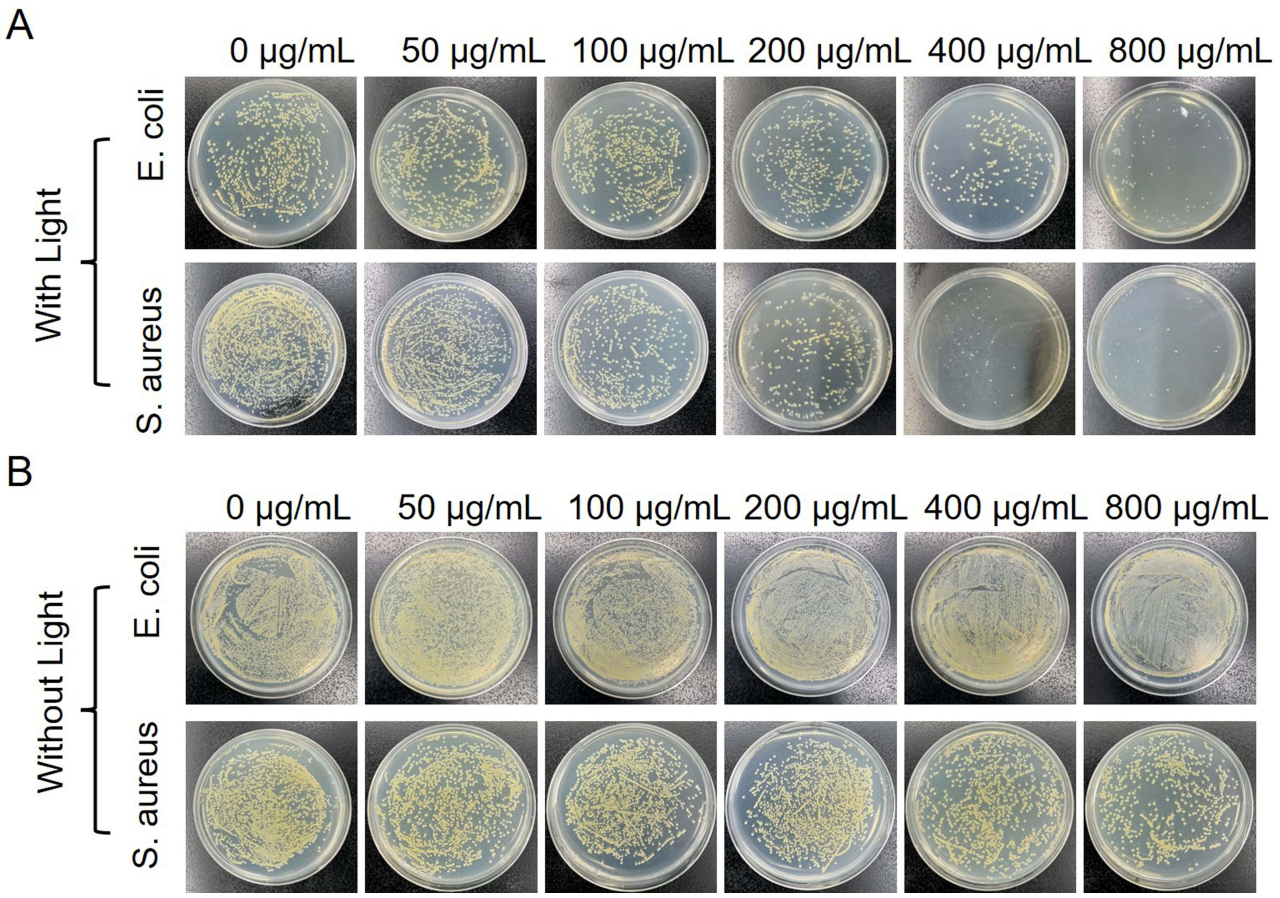

Figure 4 Images of bacterial colonies of *E. coli* and *S. aureus* treated by different concentrations of GBT with white light irradiation (**A**) or without white light irradiation (**B**).

alone could not cause ROS generation (Figure 5A). This observation suggested that bacteria treated with GBT produced a large magnitude of ROS, which further activated the oxidative stress signaling pathway and caused bacteria death.

We further observed bacterial morphological changes caused by GBT. SEM images of *E. coli* and *S. aureus* were taken to observe the morphological changes after 6-h co-incubation with GBT. The images showed that untreated *E. coli* was rod-shaped, untreated *S. aureus* was spherical, and the surface of both bacteria was smooth and intact. Treatment with GBT alone or white light did not show toxicity to the bacteria. However, the surfaces of both bacteria treated with GBT plus white light became rough and wrinkled, indicating obvious bacterial structural destruction and death of most bacteria (Figure 5B). These results indicate that ROS-mediated bacterial wall damage is the leading mechanism of the anti-bacterial effect of GBT. Overall, we demonstrate that GBT has effective anti-bacterial property under white light exposure, which may accelerate the inflammatory phase of wound healing.

The Promoting Effects of GBT on Cell Proliferation and Migration

Tissue cell proliferation and migration in the injured skin area are important to wound healing. We therefore examined whether GBT also promoted tissue cell proliferation and migration except for its bacteria-killing effect. The biocompatibility of GBT was also assessed by checking the viability of NIH-3T3 cells using CCK-8 assay after 24-h incubation with GBT. Results showed that GBT alone did not significantly affect the viability of NIH-3T3 cells (Figure 6A), suggesting that GBT has a good biosafety. We then examined the effect of GBT on the proliferation of NIH-3T3 cells using EdU assay. Treatment with GBT plus white light irradiation significantly promoted the proliferation of NIH-3T3 cells compared with the untreated cells as evidenced by the increased cell numbers (Figure 6B), indicating that GBT has a great proliferation-promoting capacity under white light exposure. We further investigated the capability of GBT in stimulating cell migration via scratch wound healing experiments in vitro. Figure 6C indicates that 3T3 cells in the GBT

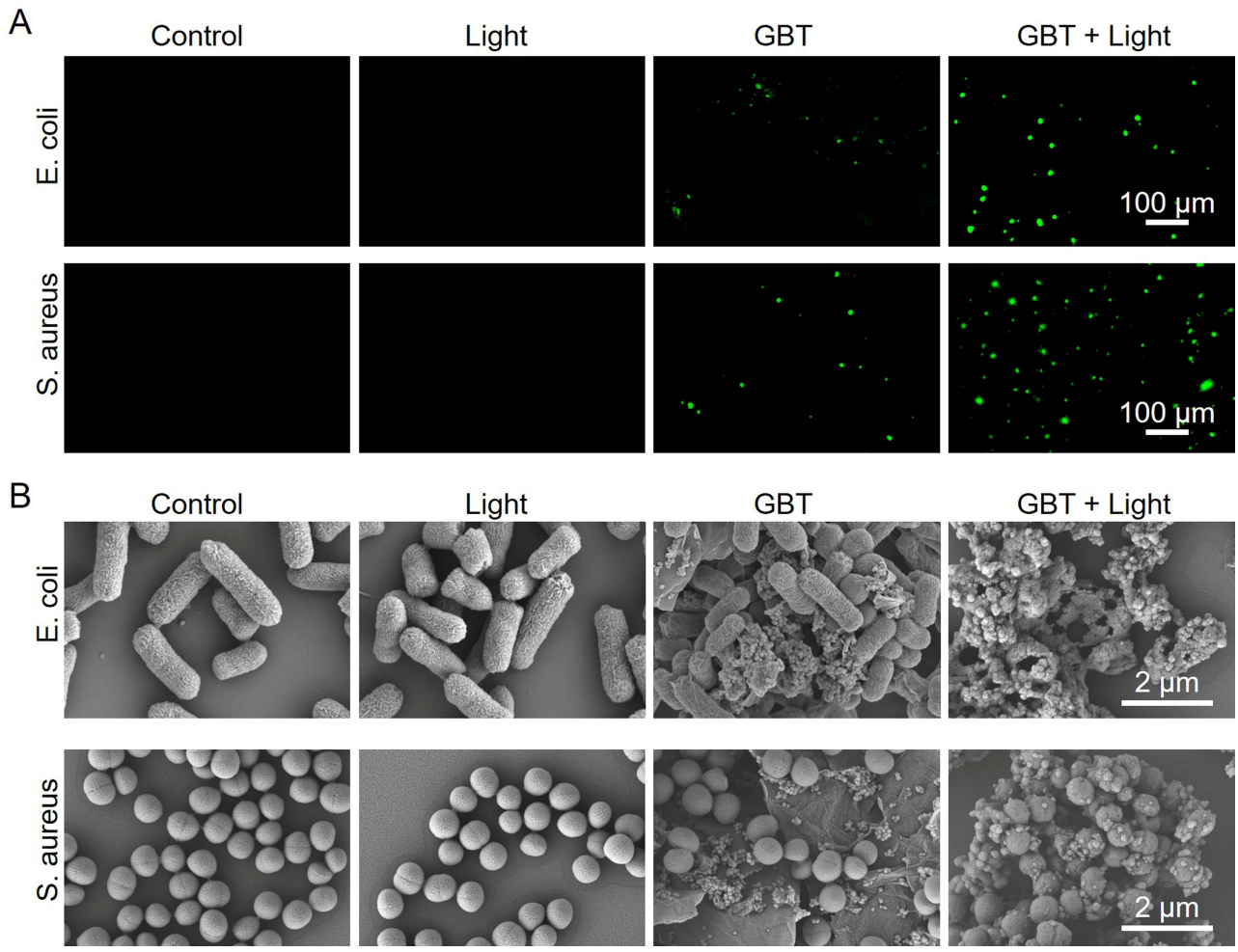

Figure 5 Evaluation on the antibacterial mechanism of GBT. (**A**) The ROS-generating ability of *E. coli* and *S. aureus* incubated with GBT with or without white light irradiation. PBS was used as a control. (**B**) SEM images of *E. coli* and *S. aureus* treated with GBT with or without white light irradiation.

group achieved a fastest scratch closure compared to the control. After incubation with GBT or PBS for 24 h, 42.3% and 16.4% of the cell migration area was formed for the GBT and control groups using further quantitative analysis by ImageJ (Figure 6D). These results indicate that GBT has a significant ability in promoting cell proliferation and migration, which favors the wound healing process.

The Promoting Effect of GBT on Skin Wound Healing in Mice in vivo

The above results showed that GBT had excellent abilities in promoting ROS generation, bacterial killing, cell migration and proliferation, and we expected that GBT could accelerate wound healing in vivo. A circular skin wound of about 1 cm wide was created by cutting on the back of female BALB/c mice (18−21 g, 4−6 weeks old), *E. coli* solution was smeared at the wound site to build the infection wound mice model and 2 h later samples were collected. After culturing for 24 h, bacterial colonies were clearly formed (Figure 7A, left), suggesting wounds were successfully infected by *E. coli*. Then, the wound was treated with PBS, light, GBT, GBT + light, respectively. The wound size was photo-filed every 2 days till the last day of treatment. The wound healing curve showed that mice in the GBT + light group showed the best wound healing effect (Figure 7B). The photographs of wound healing also consolidate that GBT + light yielded the best wound healing performance, the wound was almost healed and there were few scars left after 6-day treatment (Figure 7C), while mice in the negative control groups displayed slower wound healing, as presented by obvious scarring and the largest relative wound area (Figure 7C). To further confirm the sterilizing effect of GBT against *E. coli*-infection, bacterial samples were collected from the wounds again at day 7 and cultured in vitro. Little bacterial colonies were

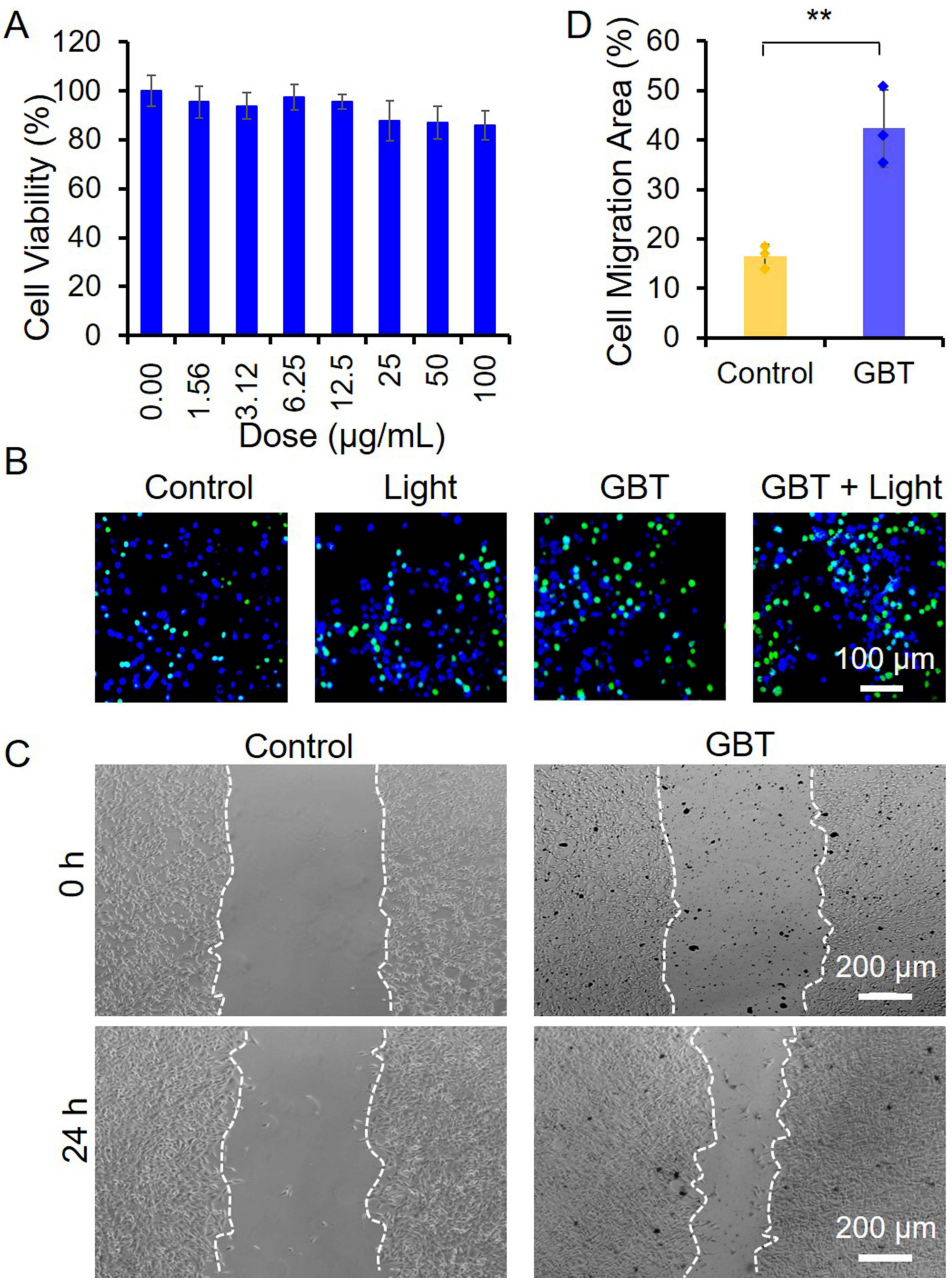

Figure 6 The cell migration- and proliferation-promoting abilities of GBT. (**A**) CCK8 assay of NIH-3T3 cells showing that GBT had no effect on cell viability. The cells were treated with different concentrations of GBT for 24 h with or without white light irradiation. (**B**) EdU stained (green) and Hoechst 33,342 stained (blue) fluorescence images of 3T3 cells treated with GBT with or without white light. (**C**) Scratch wound healing assay in vitro, which indicated that GBT significantly increased the migration of NIH-3T3 cells after incubation with GBT for 24 h. (**D**) Cell migration assay showing that GBT significantly increased the migration of NIH-3T3 cells. The percentage of cell migration area after 24 h treatment with GBT from using ImageJ analysis software ** $p < 0.01$.

formed on the culture plate with samples from GBT + Light-treated wounds, while bacterial colonies were clearly visible for *E. coli* samples from untreated or GBT treated wounds (Figure 7A, Right). These results also directly demonstrated the presence of bacterial infection at the untreated wounds all through the experiment time period, further proving the success of infection. These results indicate that GBT can accelerate wound repair in vivo.

The wound healing-promoting effect of GBT was further identified at the histological examination. At the end of the 8-day treatment, skin tissues of the wound areas were harvested, developed, sectioned, and stained with hematoxylin-eosin (H&E). H&E staining images showed that, compared with other three groups, the GBT + light group had a complete epidermis, new hair follicle regeneration, fewer inflammatory cells, and a significant reduction in scar

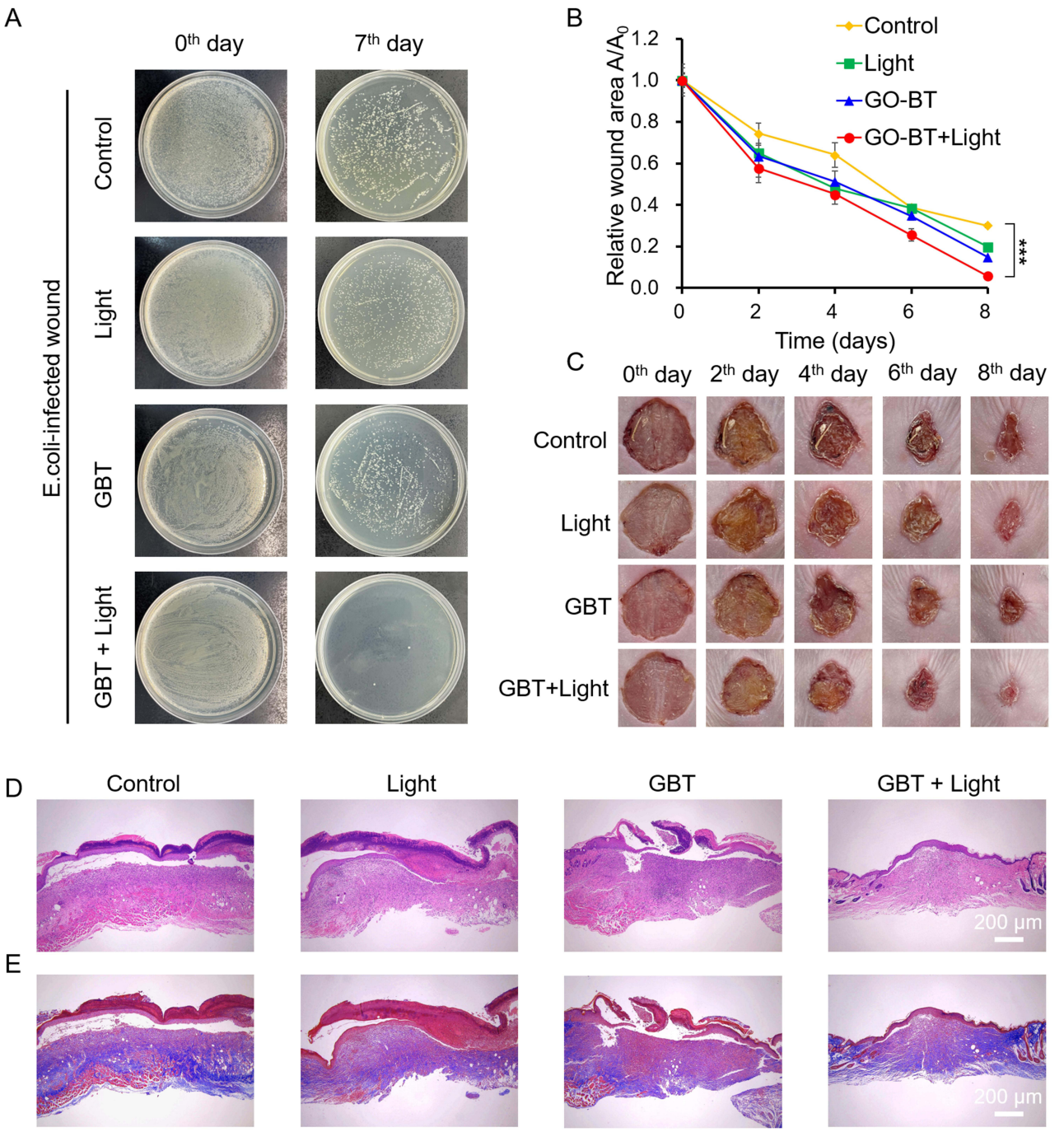

Figure 7 The wound healing-promoting effect of GBT in *E. coli*-infected mice in vivo. (**A**) Photographs of bacterial colonies collected from *E. coli*-infected wounds before and after 7 days treatment. (**B**) Relative wound areas of mice under different treatments. *** $p < 0.001$. (**C**) Representative gross views of the wounds of mice at different times during treatment. (**D**) H&E and (**E**) Masson's trichrome staining of the wound tissue sections after the treatment.

width (Figure 7D), demonstrating that GBT has an excellent wound healing capability under white light irradiation. In addition, collagen deposition encouraged cell proliferation and differentiation and was crucial for wound healing. Masson's trichrome staining was used to evaluate collagen deposition. As shown in Figure 7E, the skin tissues of GBT + Light group showed abundant collagen fiber deposition after 8 days treatment, which is much higher than in the other groups, and the collagen deposits were well organized with dense fibers. These results were consistent with previous in vitro antibacterial activity and in vivo infectious wound contraction, providing further evidence that the

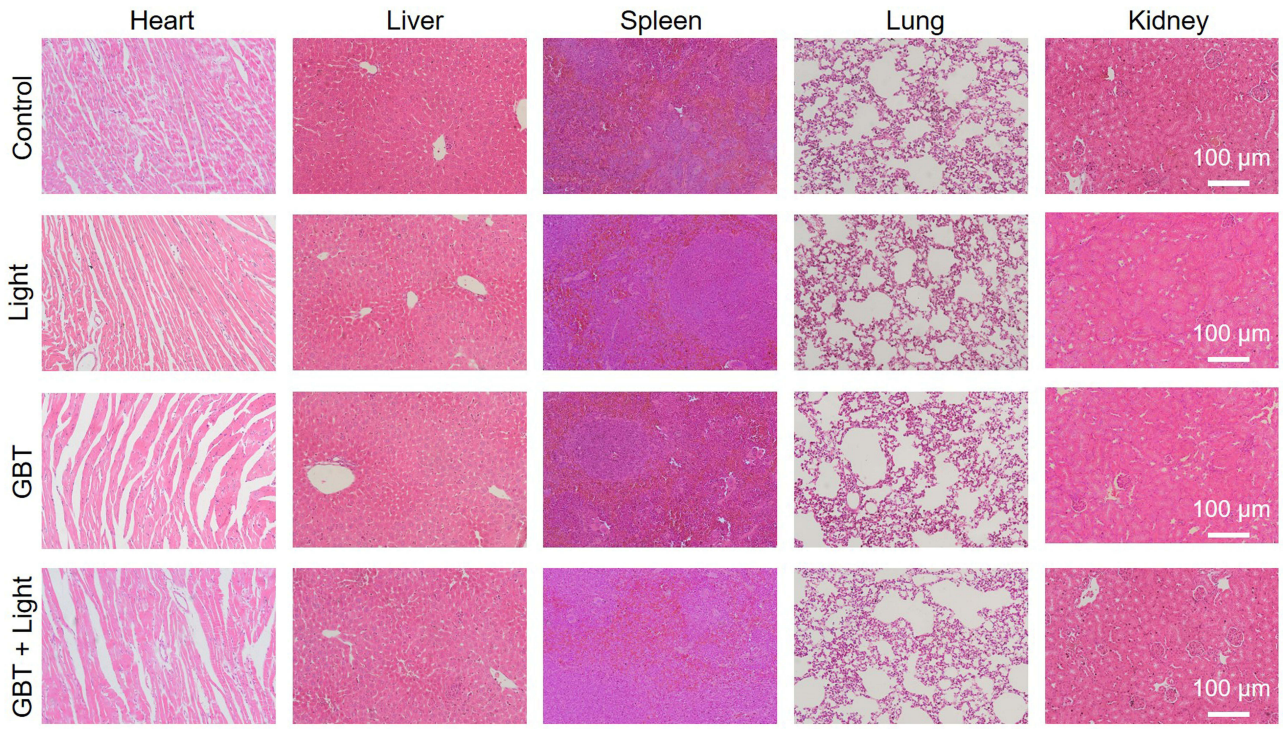

Figure 8 H&E stains of the main organs (heart, liver, spleen, lung, and kidney) after treatments with PBS, Light, GBT or GBT + light in mice.

improved antibacterial activity of GBT under white light irradiation and consequent promotion of infectious wound healing. Therefore, it could be concluded that compared to other groups, the GBT + Light group exhibited the most significant wound contraction within 8 days and achieved almost complete wound healing at a histochemical level. In conclusion, GBT + Light could promote the infectious wound healing by reducing inflammation, accelerating cell proliferation, tissue regeneration and collagen deposition.

The biosafety of GBT was further examined by observing the pathological features of vital organs. H&E stains of the major organs (heart, liver, spleen, lung and kidney) of mice showed that treatment with GBT did not induce obvious damage or destruction in these organs (Figure 8), which proved the in vivo biosafety of GBT.

The above results demonstrate that treatment with GBT plus white light irradiation could kill bacteria and promote cell proliferation and migration, tissue regeneration and collagen deposition. In this process, ROS is likely the major factor in bacterial inactivation and wound healing, as supported by the in vitro ROS assay. In addition, it can be inferred that ROS initiates cascading redox signaling, which has been reported to modulate the local cytoskeleton thereby to promote cell migration.[38]

Conclusion

In summary, we successfully fabricated GBT nanosystem with good cytocompatibility through a facile and classical amide reaction for procedural therapy of bacteria-infected wounds. The system incorporated several distinct therapeutic strategies together. At the inflammation phase, the separation of electron-hole pairs from BT and graphene could induce the production of a large amount of ROS after white light exposure which could effectively kill *E. coli* and *S. aureus* to prevent wound infection. At the proliferation phase, G acts as a scaffold to accelerate fibroblast proliferation and migration to the wound to accelerate wound healing. More importantly, in vivo infected-wound healing treated by GBT exhibited faster collagen deposition (with almost no scar formation) and accelerated regeneration of skin tissue at the end of 8 days. Overall, the study offered a facile approach to construct efficient, promising and programmable nanosystem to accelerate bacterial-infected wound healing.

Future Prospect

Due to the revelation of piezoelectricity, endogenous electric fields, and transmembrane potentials in biological tissues, researchers have developed various piezoelectric materials for biomedical applications.[39–42] As electric fields can influence tissue development and regeneration, piezoelectric materials generate electric signals when subjected to pressure, making them ideal for biological electrical activity. Electrical stimulation has been shown to promote cell growth, differentiation, and tissue regeneration, and BT is a classic piezoelectric material.[43–45] Therefore, we speculate that our synthesized GBT can also promote cell growth and tissue regeneration by electrical signals through the piezoelectric effect, accelerating wound healing. However, due to limitations in laboratory conditions, we have not conducted experiments in this area. At the same time, we also expect that GBT can be applied to repair other tissues as an intelligent system in combination with other treatments.

Acknowledgments

This work was supported by the National Natural Science Foundation of China (22007063 and 82002063), Shanxi Medical Key Science and Technology Project Plan of China (2020XM01).

Disclosure

The authors report no conflicts of interest in this work.

References

1. Rajendran NK, Kumar SSD, Houreld NN, Abrahamse H. A review on nanoparticle based treatment for wound healing. *J Drug Deliv Sci Technol*. 2018;44:421–430. doi:10.1016/j.jddst.2018.01.009
2. Berthet M, Gauthier Y, Lacroix C, Verrier B, Monge C. Nanoparticle-based dressing: the future of wound treatment? *Trends Biotechnol*. 2018;36(1):119. doi:10.1016/j.tibtech.2017.08.007
3. Gurtner GC, Werner S, Barrandon Y, Longaker MT. Wound repair and regeneration. *Nature*. 2008;453(7193):314–321. doi:10.1038/nature07039
4. Meddahi-Pellé A, Legrand A, Marcellan A, et al. Organ repair, hemostasis, and in vivo bonding of medical devices by aqueous solutions of nanoparticles. *Angew Chem Int Ed Engl*. 2014;53(25):6369–6373. doi:10.1002/anie.201401043
5. Singer AJ, Clark RA. Cutaneous wound healing. *N Engl J Med*. 1999;341(10):738–746. doi:10.1056/NEJM199909023411006
6. Werner S, Grose R. Regulation of wound healing by growth factors and cytokines. *Physiol Rev*. 2003;83(3):835–870. doi:10.1152/physrev.2003.83.3.835
7. Shechter R, Schwartz M. CNS sterile injury: just another wound healing? *Trends Mol Med*. 2013;19(3):135–143. doi:10.1016/j.molmed.2012.11.007
8. Chang Y, Cheng Y, Feng Y, et al. Upshift of the d band center toward the fermi level for promoting silver ion release, bacteria inactivation, and wound healing of alloy silver nanoparticles. *ACS Appl Mater Interfaces*. 2019;11(13):12224–12231. doi:10.1021/acsami.8b21768
9. Singh V, Kashyap S, Yadav U, et al. Nitrogen doped carbon quantum dots demonstrate no toxicity under in vitro conditions in a cervical cell line and in vivo in Swiss albino mice. *Toxicol Res*. 2019;8(3):395–406. doi:10.1039/C8TX00260F
10. Wu H, Li F, Wang S, et al. Ceria nanocrystals decorated mesoporous silica nanoparticle based ROS-scavenging tissue adhesive for highly efficient regenerative wound healing. *Biomaterials*. 2018;151:66–77. doi:10.1016/j.biomaterials.2017.10.018
11. Xiao J, Chen S, Yi J, Zhang H, Ameer GA. A cooperative copper metal-organic framework-hydrogel system improves wound healing in diabetes. *Adv Funct Mater*. 2017;27(1):1604872. doi:10.1002/adfm.201604872
12. Li M, Aveyard J, Doherty KG, et al. Antimicrobial nitric oxide-releasing electrospun dressings for wound healing applications. *ACS Mater Au*. 2022;2(2):190–203. doi:10.1021/acsmaterialsau.1c00056
13. Wu M, Lu Z, Wu K, et al. Recent advances in the development of nitric oxide-releasing biomaterials and their application potentials in chronic wound healing. *J Mater Chem B*. 2021;9(35):7063–7075. doi:10.1039/D1TB00847A
14. Wu M, Zhang Z, Liu Z, et al. Piezoelectric nanocomposites for sonodynamic bacterial elimination and wound healing. *Nano Today*. 2021;37:101104. doi:10.1016/j.nantod.2021.101104
15. Feng Y, Wang J, Ning X, et al. BaTiO3@Au nanoheterostructure suppresses triple-negative breast cancer by persistently disrupting mitochondrial energy metabolism. *Nano Research*. 2023;16(2):2775–2785. doi:10.1007/s12274-022-4927-9
16. Kim CO, Kim S, Shin DH, et al. High photoresponsivity in an all-graphene p-n vertical junction photodetector. *Nat Commun*. 2014;5:3249. doi:10.1038/ncomms4249
17. Chen Z, Wang Z, Gu Z. Bioinspired and Biomimetic Nanomedicines. *Acc Chem Res*. 2019;52(5):1255–1264. doi:10.1021/acs.accounts.9b00079
18. Huang H, He Y, Li X, et al. Bi 2 O 2 (OH)(NO 3) as a desirable [Bi 2 O 2] 2+ layered photocatalyst: strong intrinsic polarity, rational band structure and {001} active facets co-beneficial for robust photooxidation capability. *J Mater Chem a Mater*. 2015;3(48):24547–24556. doi:10.1039/C5TA07655B
19. Ji H, Sun H, Qu X. Antibacterial applications of graphene-based nanomaterials: recent achievements and challenges. *Adv Drug Deliv Rev*. 2016;105(Pt B):176–189. doi:10.1016/j.addr.2016.04.009
20. Tu Y, Lv M, Xiu P, et al. Destructive extraction of phospholipids from Escherichia coli membranes by graphene nanosheets. *Nat Nanotechnol*. 2013;8(8):594–601. doi:10.1038/nnano.2013.125
21. Chen J, Peng H, Wang X, et al. Graphene oxide exhibits broad-spectrum antimicrobial activity against bacterial phytopathogens and fungal conidia by intertwining and membrane perturbation. *Nanoscale*. 2014;6(3):1879–1889. doi:10.1039/C3NR04941H

22. Mao J, Guo R, Yan LT. Simulation and analysis of cellular internalization pathways and membrane perturbation for graphene nanosheets. *Biomaterials*. 2014;35(23):6069–6077. doi:10.1016/j.biomaterials.2014.03.087
23. Li Y, Yuan H, von Dem Bussche A, et al. Graphene microsheets enter cells through spontaneous membrane penetration at edge asperities and corner sites. *Proc Natl Acad Sci USA*. 2013;110(30):12295–12300. doi:10.1073/pnas.1222276110
24. Ye S, Shao K, Li Z, et al. Antiviral activity of graphene oxide: how sharp edged structure and charge matter. *ACS Appl Mater Interfaces*. 2015;7(38):21571–21579. doi:10.1021/acsami.5b06876
25. Li J, Wang G, Zhu H, et al. Antibacterial activity of large-area monolayer graphene film manipulated by charge transfer. *Sci Rep*. 2014;4:4359. doi:10.1038/srep04359
26. Gurunathan S, Han JW, Dayem AA, Eppakayala V, Kim JH. Oxidative stress-mediated antibacterial activity of graphene oxide and reduced graphene oxide in Pseudomonas aeruginosa. *Int J Nanomedicine*. 2012;7:5901–5914. doi:10.2147/IJN.S37397
27. Guo Z, Zhang P, Xie C, et al. Defining the surface oxygen threshold that switches the interaction mode of graphene oxide with bacteria. *ACS Nano*. 2023;17(7):6350–6361. doi:10.1021/acsnano.2c10961
28. Chong Y, Ge C, Fang G, et al. Light-enhanced antibacterial activity of graphene oxide, mainly via accelerated electron transfer. *Environ Sci Technol*. 2017;51(17):10154–10161. doi:10.1021/acs.est.7b00663
29. Kim SE, Kim MS, Shin YC, et al. Cell migration according to shape of graphene oxide micropatterns. *Micromachines*. 2016;7(10):186. doi:10.3390/mi7100186
30. Thangavel P, Kannan R, Ramachandran B, et al. Development of reduced graphene oxide (rGO)-isabgol nanocomposite dressings for enhanced vascularization and accelerated wound healing in normal and diabetic rats. *J Colloid Interface Sci*. 2018;517:251–264. doi:10.1016/j.jcis.2018.01.110
31. Ryoo SR, Kim YK, Kim MH, Min DH. Behaviors of NIH-3T3 fibroblasts on graphene/carbon nanotubes: proliferation, focal adhesion, and gene transfection studies. *ACS Nano*. 2010;4(11):6587–6598. doi:10.1021/nn1018279
32. Cheng Y, Chang Y, Feng Y, et al. Simulated sunlight-mediated photodynamic therapy for melanoma skin cancer by titanium-dioxide-nanoparticle-gold-nanocluster-graphene heterogeneous nanocomposites. *Small*. 2017;13(20):1603935. doi:10.1002/smll.201603935
33. Lin F, Du F, Huang J, et al. Substrate effect modulates adhesion and proliferation of fibroblast on graphene layer. *Colloids Surf B Biointerfaces*. 2016;146:785–793. doi:10.1016/j.colsurfb.2016.07.008
34. Hummers WS, Offeman RE. Preparation of graphitic oxide. *J Am Chem Soc*. 1958;80(6):1339. doi:10.1021/ja01539a017
35. Applerot G, Lellouche J, Lipovsky A, et al. Understanding the antibacterial mechanism of CuO nanoparticles: revealing the route of induced oxidative stress. *Small*. 2012;8(21):3326–3337. doi:10.1002/smll.201200772
36. Cheng Y, Chang Y, Feng Y, et al. Hierarchical acceleration of wound healing through intelligent nanosystem to promote multiple stages. *ACS Appl Mater Interfaces*. 2019;11(37):33725–33733. doi:10.1021/acsami.9b13267
37. Wang L, Hussain Z, Zheng P, et al. A mace-like heterostructural enriched injectable hydrogel composite for on-demand promotion of diabetic wound healing. *J Mater Chem B*. 2023;11(10):2166–2183. doi:10.1039/D2TB02403A
38. Dickinson BC, Chang CJ. Chemistry and biology of reactive oxygen species in signaling or stress responses. *Nat Chem Biol*. 2011;7(8):504–511. doi:10.1038/nchembio.607
39. Cai C, Zhang X, Li Y, et al. Self-Healing hydrogel embodied with macrophage-regulation and responsive-gene-silencing properties for synergistic prevention of peritendinous adhesion. *Adv Mater*. 2022;34(5):2106564. doi:10.1002/adma.202106564
40. Montoya C, Du Y, Gianforcaro AL, et al. On the road to smart biomaterials for bone research: definitions, concepts, advances, and outlook. *Bone Res*. 2021;9(1):12.
41. Zhao D, Feng PJ, Liu JH, et al. Electromagnetized-nanoparticle-modulated neural plasticity and recovery of degenerative dopaminergic neurons in the mid-brain. *Adv Mater*. 2020;32(43):2003800. doi:10.1002/adma.202003800
42. Liu Y, Dzidotor G, Le TT, et al. Exercise-induced piezoelectric stimulation for cartilage regeneration in rabbits. *Sci Transl Med*. 2022;14(627):eabi7282. doi:10.1126/scitranslmed.abi7282
43. Zhou L, Yuan T, Jin F, et al. Advances in applications of piezoelectronic electrons in cell regulation and tissue regeneration. *J Mater Chem B*. 2022;10(43):8797–8823.
44. Thrivikraman G, Boda SK, Basu B. Unraveling the mechanistic effects of electric field stimulation towards directing stem cell fate and function: a tissue engineering perspective. *Biomaterials*. 2018;150:60–86. doi:10.1016/j.biomaterials.2017.10.003
45. Selvarajan S, Alluri NR, Chandrasekhar A, Kim SJ. Unconventional active biosensor made of piezoelectric BaTiO3 nanoparticles for biomolecule detection. *Sens Actuators B Chem*. 2017;253:1180–1187. doi:10.1016/j.snb.2017.07.159